RSC Medicinal Chemistry

ROYAL SOCIETY OF CHEMISTRY

RESEARCH ARTICLE

View Article Online
View Journal | View Issue

Cite this: *RSC Med. Chem.*, 2023, **14**, 1743

Dual FLT3/haspin kinase inhibitor based on 3*H*-pyrazolo[4,3-*f*]quinoline scaffold with activities against acute myeloid leukemia†

Allison L. Kempen, [a] Nickolas R. Brauer [a] and Herman O. Sintim *[abc]

Received 23rd April 2023,
Accepted 5th July 2023

DOI: 10.1039/d3md00192j

rsc.li/medchem

The 3*H*-pyrazolo[4,3-*f*]quinoline core, a privileged fusion moiety from quinoline and indazole, facilely synthesized in a one flask multi-component Doebner–Povarov reaction, is a newly described kinase hinge binder. Previous works have demonstrated that the 3*H*-pyrazolo[4,3-*f*]quinoline moiety can be tuned, *via* judicious substitution patterns, to selectively inhibit cancer-associated kinases, such as FLT3 and haspin. A first generation 3*H*-pyrazolo[4,3-*f*]quinoline-based haspin inhibitor, HSD972, and FLT3 inhibitor, HSD1169, were previously disclosed as inhibitors of various cancer cell lines. Given the recent revelation that haspin is over-expressed and plays critical proliferative roles in many cancers, and compounds with dual activity against FLT3 and other important kinases are now being actively developed by many groups, we became interested in optimizing the 3*H*-pyrazolo[4,3-*f*]quinoline-based compounds to improve activity against both FLT3 and haspin. Herein, we report the discovery of new 3*H*-pyrazolo[4,3-*f*]quinoline-based dual FLT3/haspin inhibitor, HSK205. HSK205 has remarkable potencies against FLT3-driven AML cell lines, inhibiting proliferation with GI_{50} values between 2–25 nM. Western blot analyses of treated AML cells confirm that HSK205 inhibit the phosphorylation of both FLT3 and histone H3 (a haspin target) in cells. While multi-component reactions (MCRs) have been used to make many bioactive molecules, there are very few examples of using MCRs to make compounds that target protein kinases, which have emerged as one of the top drug candidates (especially in oncology). This work highlights our recent efforts to make ultrapotent protein kinase inhibitors using multi-component reactions (especially the Doebner–Povarov reaction).

1. Introduction

Acute myeloid leukemia (AML) is a devastating disease that affects over 20 000 people in the US each year.[1] About 30% of AML patients harbor mutations in the FLT3 kinase, and for these patients, the prognosis is usually poorer than those without FLT3 mutation.[2] Many FLT3 inhibitors have been developed and trialed in the clinic and a few, including midostaurin, quizartinib, and gilteritinib, have been approved in the United States or Japan. These FLT3 inhibitors have moderately improved the survival of FLT3-harboring AML patients, although resistance to the approved FLT3 inhibitors has been observed in the clinic. Specifically, FLT3-F691I is resistant to midostaurin while FLT3-F691L is resistant to gilteritinib and quizartinib.[3] In addition to FLT3 resistant mutations, FLT3-independent resistance pathways, such as NRAS activation or mutations of other kinases, also emerge after prolonged FLT3i treatment.[4,5] In some instances, patients who were initially FLT3-positive become FLT3-negative during treatment; yet the cancer progresses, fueled by alternative pathways.[6] Thus, there is a need for newer drugs that can deal with FLT3, as well as other oncogenic pathways that may arise during treatment. Others have recently disclosed FLT3 inhibitors that have activities against other cancer related kinases, such as dual FLT3/MERTK,[7] FLT3/MNK,[8] FLT3/CDK,[9] FLT3/TOPK,[10] FLT3/PIM,[11] or FLT3/AURKA inhibitors,[12] and in these cases the authors have argued that the concurrent inhibition of the FLT3 and other kinase pathways confer some advantages in overcoming resistance. For example, CCT245718, a dual FLT3/Aurora A inhibitor could overcome FLT3-D835Y-mediated resistance.[13] In another interesting report, it was shown that the frequency of resistance to a dual FLT3/CDK4 inhibitor (AMG 925) was less than other FLT3 inhibitors (such as quizartinib) that did not inhibit CDK4.[14] Considering these prior dual inhibitors, we became interested in identifying FLT3 inhibitors that also inhibited other kinases which play important roles in cancer progression. Haspin has emerged as an interesting novel

[a] *Department of Chemistry, Purdue University, 560 Oval Drive, West Lafayette, IN 47907, USA. E-mail: hsintim@purdue.edu*
[b] *Purdue Institute for Drug Discovery, 720 Clinic Drive, West Lafayette, IN 47907, USA*
[c] *Purdue Institute for Cancer Research, 201 S. University St., West Lafayette, IN 47907, USA*

† Electronic supplementary information (ESI) available. See DOI: https://doi.org/10.1039/d3md00192j

target in cancer and is the main kinase that phosphorylates histone H3 at T3.[15] A recent preliminary report indicated that reduction of haspin *via* genetic means or inhibition by a compound reduced leukemia proliferation.[16]

Our laboratory has previously shown that the "fusion" of two known kinase hinge binders, indazole and quinoline, which are commonly found in FDA-approved drugs, such as axitinib and erlotinib, leads to the novel 3*H*-pyrazolo[4,3-*f*]quinoline (Fig. 1A), which binds to the hinge region of kinases.[17] Remarkably, the substituent at position 7 of the 3*H*-pyrazolo[4,3-*f*]quinoline moiety dictates which kinases are potently inhibited. For example, pyrazole substitution at position 7 leads to inhibitors that bind to mutant FLT3 with picomolar K_d values,[18] while phenyl boronic acid substituents lead to ultrapotent ROCK1/2 inhibitors[19] (Fig. 1B). Benzo[*d*]thiazolyl substituted compounds like HSD992 are potent CDK inhibitors,[20] while phenol containing compounds, such as HSD972, are excellent haspin inhibitors (HSD972 haspin IC_{50} = 14 nM).[21] In addition to the 3*H*-pyrazolo[4,3-*f*]quinoline core, others have shown that analogous systems, such as pyrazolo[3,4-*h*]quinoline scaffold, also have anticancer activities.[22]

Considering that HSD972 and HSD1169 (see Fig. 1), both containing the 3*H*-pyrazolo[4,3-*f*]quinoline moiety inhibit haspin or FLT3 respectively, we wondered if we could find a C7 substituent that would endow dual FLT3 and haspin kinase inhibition. Indeed, we discovered that replacement of the phenol moiety at position-7 of HSD972 with benzamide led to compound HSD1217 (Fig. 2A), which inhibited haspin more potently than our previously disclosed compound, HSD972. Thus, we became interested in optimizing HSD1217.

Analysis of the docked structure of HSD1217 to haspin (Fig. 2A) indicated that the benzamide–NH_2 moiety had a hydrogen bonding interaction with key residue D687 and was positioned towards a region harboring H651 and D649 residues, which bind to the ATP phosphate moiety. Thus, we rationalized that appending polar groups, such as imidazole, with hydrogen bonding and hydrogen donating capabilities to the benzamide that could reach the either H651 or D649 residues while maintaining hydrogen bonding with the D687 residue could provide additional interactions to increase ligand affinity for the protein. Because H651, D649, or D687 are critical for ATP binding to haspin, we speculate that inhibitors that engage these residues would have a higher chance of resisting kinase mutations that abrogate inhibitor binding.[23] *In silico* analysis of compounds **4**, **5**, and **6** (analogs of HSD1217), which contain the imidazole moiety, indicated that all three compounds could form key interactions with at least one of these ATP-binding residues (Fig. 2B–D). For docking analysis of 3*H*-pyrazolo[4,3-*f*]quinoline-based compounds to FLT3, the reader is referred to our previous publication, ref. 17.

With these preliminary compounds in hand, we began a structure–activity relationship (SAR) study to explore how modifications affected haspin and/or FLT3 inhibition. Herein, we disclose the identification of new imidazoyl-containing pyrazolo-based compounds that are dual FLT3/haspin inhibitors, inhibiting both kinases at ultra-low (sub-nanomolar) concentrations.

2. Results and discussion

2.1 Chemistry

Multicomponent reactions (MCRs) have often been utilized to rapidly synthesize a vast range of highly functionalized analogs in a single pot to build libraries for biological screening. In this work, compounds were synthesized using the Doebner-like MCR followed by subsequent amidation (Scheme 1). For our pilot library, we focused on using amines bearing imidazole or bioisosteres thereof as we believed that such heterocyclic amines that are found in other drugs, such as nilotinib, could facilitate ligand engagement with protein residues, *vide supra*. During the Doebner-like MCR, the amine and aldehyde react to form the Schiff base, which subsequently reacts with the added ketone in the presence of the acid catalyst (HCl). With the MCR product A (see Scheme 1) in hand, the final amide products (**4–15**) were

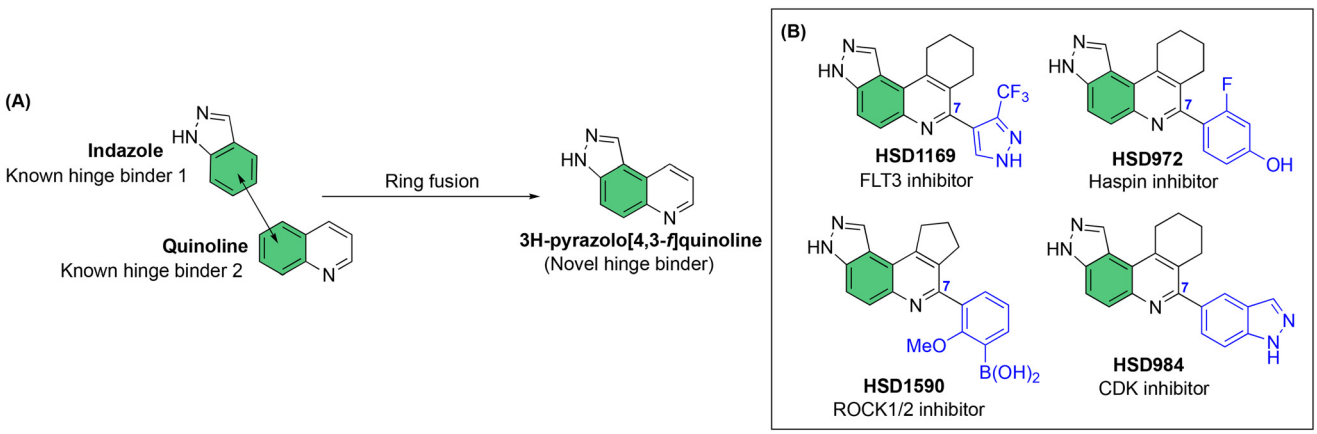

Fig. 1 A) Fusion of indazole with quinoline to afford the novel hinge binder, 3*H*-pyrazolo[4,3-*f*]quinoline core. B) C-7 substitution of the 3*H*-pyrazolo[4,3-*f*]quinoline moiety affects kinase targeting.

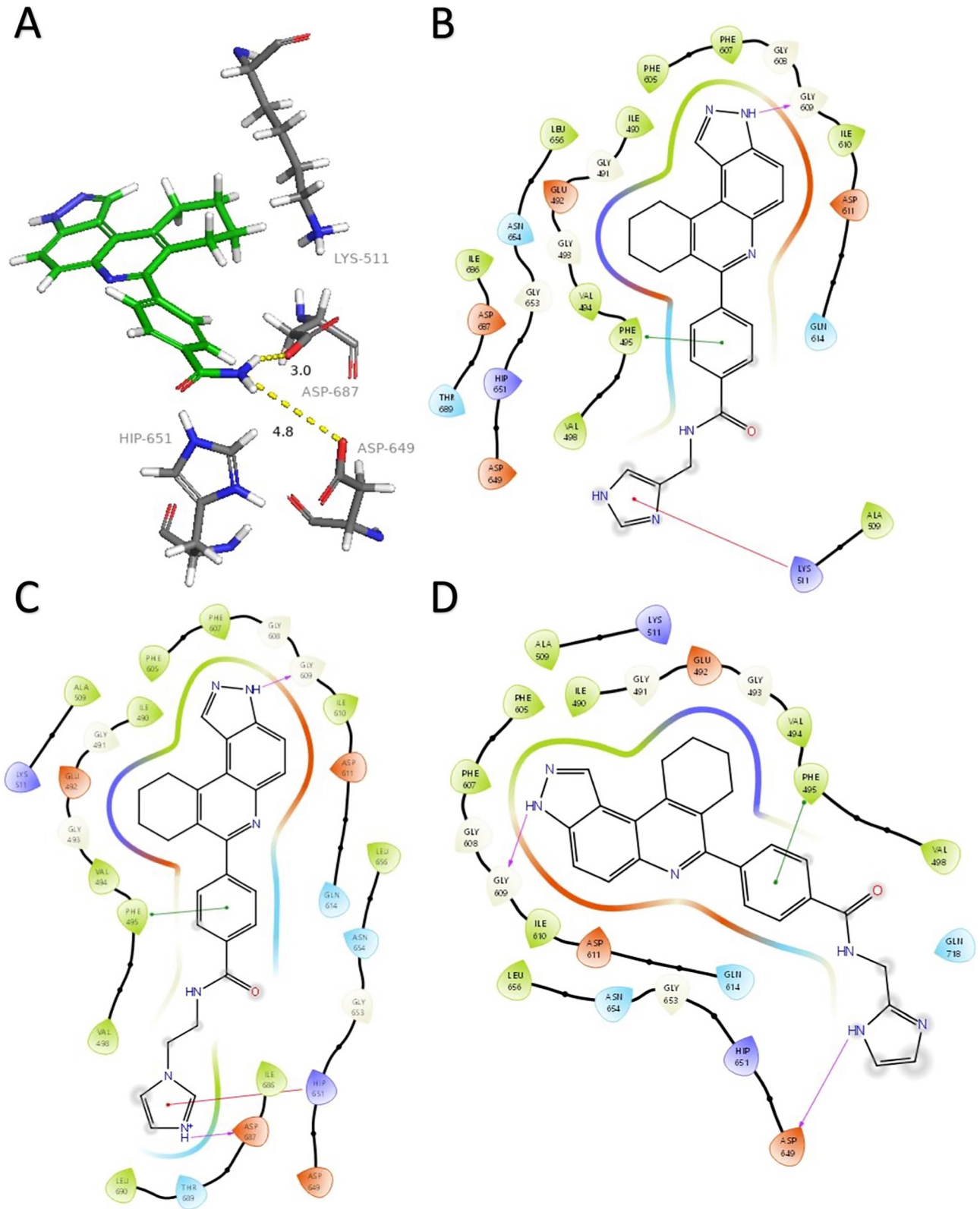

Fig. 2 A) HSD1217 and ATP-binding residues. Docked structures showing interactions between haspin (PDB: 2WB8) and three initial compounds (B) **4**, (C) **5**, and (D) **6**. Hydrogen bonds are represented in fuchsia, pi–cation interactions in red, and pi–pi stacking in green. Solvent exposure is represented with gray rings surrounding atoms. Docking was performed using Glide (Schrödinger) and visualization through PyMol and Maestro.

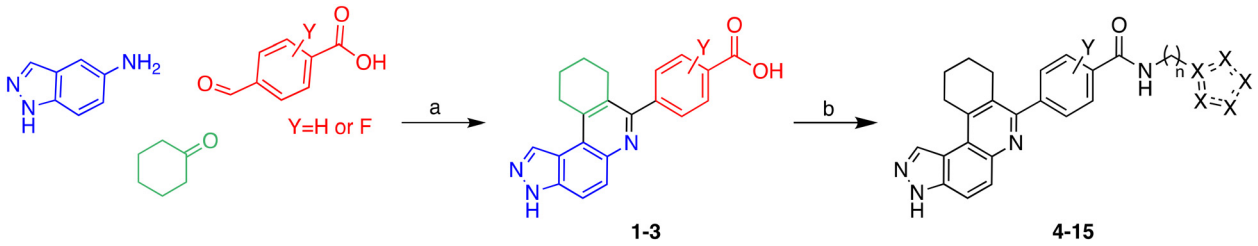

Scheme 1 Synthesis of analogs *via* Doebner-like MCR followed by amidation. (a) EtOH, reflux, 2 h, then ketone (2 equiv.), cat. HCl, reflux, 12 h; (b) HATU, DIPEA, DMF, 60 °C, 12 h.

formed *via* amidation, using commercially available amines, HATU and Hünig's base.

2.2 Kinase assay and structure–activity relationship (SAR) study

With the amide kinase inhibitor library in hand, we began by analyzing kinase inhibition as well as AML cell line (Molm-14, which harbors FLT3-ITD, and MV4-11) growth inhibition at 50 nM compound concentration (Table 1).

All compounds were screened in lab against haspin and FLT3 using the ADP Glo Kinase Assay (Promega, Madison, WI). Compounds were screened at a concentration of 50 nM, and HSD1169 and gilteritinib were used as positive controls. Additionally, cellular growth inhibition of the analogs was evaluated against two AML cell lines, Molm-14 (FLT3-ITD) and MV4-11.

The structure–activity relationship (SAR) study demonstrated that the imidazole ring is critical for activity against both haspin and FLT3, as even subtle modifications dramatically affected kinase inhibition. Compounds **4**, **5** and **6** all contain the imidazole moiety, albeit substituted differently; their inhibition profiles against the tested kinases are however different. Compound **6**, the 2-substituted imidazole, inhibited haspin and FLT3 (77% and 76%, respectively) better than **5**, the 1-substituted imidazole, (33% and 31%, respectively), and **4**, the 4-substituted imidazole (54% and 49%, respectively). Considering that compound **6** showed the best inhibitions of the tested kinases, we became interested in exploring how substitution patterns on **6** could potentially improve potency. Substituting the –NH on compound **6** with –NMe, as in compound **7**, reduced haspin and FLT3 inhibition as well as AML growth inhibition. For example, while at 50 nM, compound **6** inhibited haspin at 77%, the –NMe analog **7** inhibited the same enzyme at 26%. For FLT3, potency dropped from 76% inhibition with compound **6** at 50 nM to only 14% inhibition with compound **7**. Replacing the imidazole unit in compound **6** with other 5-membered bioisosteres (triazole (**8**), tetrazole (**10**) or thiazole (**13**)) afforded compounds that could inhibit both kinases and AML cell proliferation, but generally less so than compound **6**. Extending the length of carbon chain between the amide and the imidazole by one unit to give compound **15** did not drastically impact inhibition of either kinase.

We routinely explore the effects of fluorine substitution on lead compounds as it is known that fluorine can be used to tune drug properties (both target engagement as well as general drug properties, such as metabolic stability).[24] Thus, we explored fluorinating the benzamide moiety of compound **6** to afford compounds **9** and **11** but FLT3 and haspin kinase inhibitions were not significantly impacted (compare compounds **9** and **11** with **6**, Table 1). Some imidazole-containing drugs, such as nilotinib, have the imidazole unit methylated at position 4. Thus, we also wanted to investigate the extent that methylation of the imidazole unit in compound **6** would affect kinase inhibition. To our delight, this significantly improved potency against haspin, FLT3, and AML cell proliferation. Compound **14** (also called HSK205) at only 50 nM inhibited haspin and FLT3 at 97% and 94%, respectively, hinting that this compound could be an ultra-potent inhibitor of both FLT3 and haspin (*vide infra*). Indeed, at only 50 nM, compound HSK205 almost completely inhibited (96% and 94%, respectively) the growth of Molm-14 (FLT3-ITD) and MV4-11 cells.

To validate results obtained in our laboratory, we also sent HSK205 to contract research organizations, Eurofins and Reaction Biology, to obtain binding data for haspin (Eurofins) and enzyme inhibition data for FLT3 (Reaction Biology). At 10 μM ATP, HSK205 inhibited the FLT3-ITD enzyme with an IC_{50} = 0.199 nM, while under similar conditions, gilteritinib had an IC_{50} = 0.121 nM (Fig. 3A). For the mutated FLT3 D835Y enzyme, HSK205 inhibited with an IC_{50} = 0.187 nM, whereas gilteritinib had an IC_{50} = 0.024 nM. With regards to haspin inhibition, HSK205 could bind to haspin with K_d = 0.55 nM (K_d of control haspin inhibitor CHR-6494 < 0.17 nM), Fig. 3C. This SAR study has validated earlier reports that the 3*H*-pyrazolo[4,3-*f*]quinoline moiety can target FLT3 and the moiety is highly tunable, in that substitution at the C7 position can be used to target other kinases. For example, HSD1169, also a 3*H*-pyrazolo[4,3-*f*] quinoline-containing compound and bearing a fluorinated pyrazole is a strong inhibitor of FLT3 but a weak inhibitor of haspin, while changing the C7 moiety to a benzamide leads to a dual FLT3/haspin inhibitor.

2.3 Target engagement and *in vitro* biological activity

We proceeded to evaluate if HSK205 does indeed inhibit haspin in AML cells and performed immunoblotting to confirm inhibition of histone H3 (Thr3) phosphorylation by haspin (Fig. 4A). Molm-14 cells were treated with either

Table 1 Structures of compounds evaluated, kinase inhibition, and cellular growth inhibition data. Haspin and FLT3 inhibition were evaluated in-house *via* ADP Glo Kinase Assay. All compounds were screened against kinases and Molm-14 and MV4–11 cells at a concentration of 50 nM. Values reported are means of triplicates

		Percent inhibition (%) at 50 nM inhibitor conc.						Percent inhibition (%) at 50 nM inhibitor conc.			
Compound	Structure	Haspin	FLT3	MOLM-14	MV4-11	Compound	Structure	Haspin	FLT3	MOLM-14	MV4-11
4	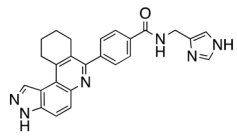	54 ± 1	49 ± 6	67 ± 3	62 ± 9	**11**	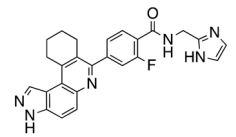	76 ± 4	85 ± 9	80 ± 3	82 ± 5
5	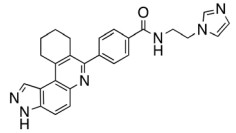	33 ± 4	31 ± 2	42 ± 6	35 ± 5	**12**	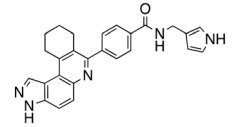	41 ± 8	46 ± 2	39 ± 11	28 ± 6
6	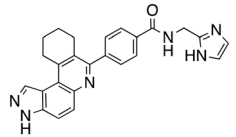	77 ± 3	76 ± 7	84 ± 5	80 ± 10	**13**	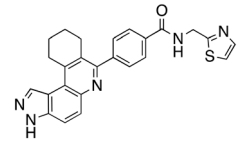	68 ± 6	53 ± 7	55 ± 5	60 ± 2
7	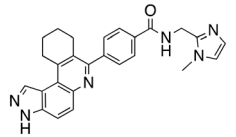	26 ± 2	14 ± 4	21 ± 7	25 ± 4	**14** (HSK205)	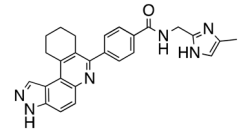	97 ± 2	94 ± 3	96 ± 4	94 ± 7
8	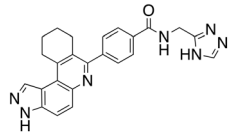	57 ± 8	49 ± 1	48 ± 4	52 ± 7	**15**	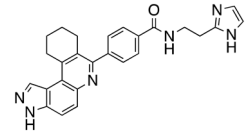	78 ± 3	71 ± 9	73 ± 8	69 ± 1
9	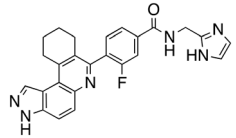	53 ± 2	88 ± 5	87 ± 9	79 ± 4	**HSD1169**	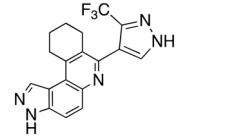	39 ± 10	81 ± 2	90 ± 5	92 ± 4
10	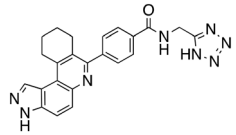	57 ± 2	51 ± 3	50 ± 1	41 ± 8	**Gilteritinib**	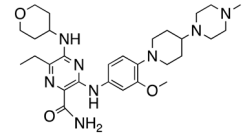	11 ± 4	93 ± 4	87 ± 6	91 ± 5

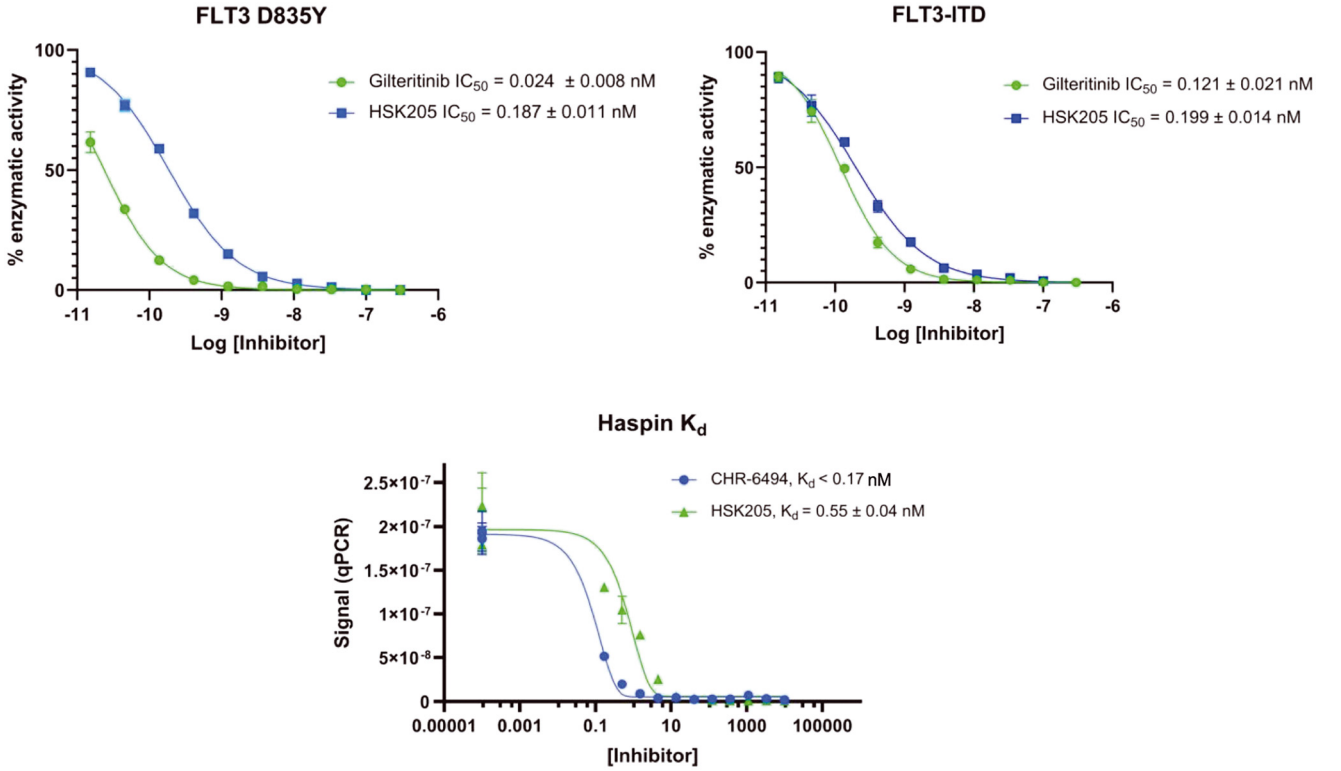

Fig. 3 Enzyme binding and inhibition data. Compounds were tested against FLT3-ITD enzyme in 10-dose IC_{50} duplicate mode with a 3-fold serial dilution starting at 10 μM. Compounds were tested against FLT3 (D835Y) enzyme in 10-dose IC_{50} duplicate mode with a 3-fold serial dilution starting at 10 μM. K_d data for haspin kinase obtained by Eurofins. Each data point represents the mean and error bars represent the SEM of triplicates. All data was fitted to a non-linear regression equation using GraphPad Prism 9.0 software.

HSK205 (5 nM or 20 nM or 100 nM) or DMSO control or gilteritinib (a negative control) at the higher 100 nM concentration, and cells were harvested after 24 hours of treatment. The samples were subsequently analyzed for the phosphorylation of histone H3 (Thr3) by haspin.

Results showed that HSK205 was effective in reducing phosphorylation of histone H3 (Thr3), with a more pronounced effect at 20 nM compared to 5 nM and 100 nM compared to 20 nM (Fig. 4B). Gilteritinib, however, did not display haspin inhibition in Molm-14 cells.

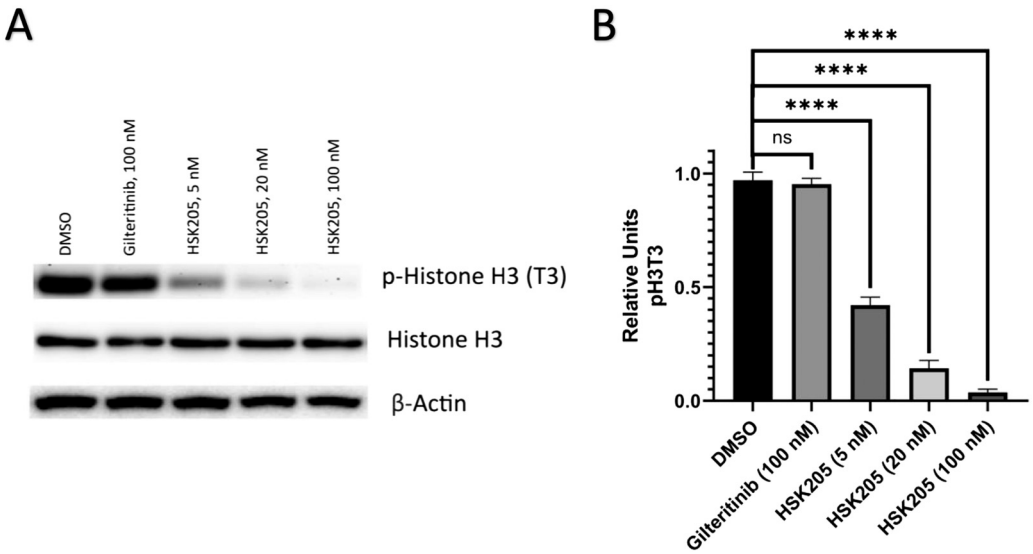

Fig. 4 Western blot analysis. (A) Molm-14 cells were treated with HSK205 (5, 20, or 100 nM) or control for 24 hours. Gilteritinib at 100 nM was used as a positive control. (B) Bands were quantified relative actin loading control. Values are reported as means of triplicates and error bars represent standard deviation (NS: $p > 0.05$, *: $p < 0.05$, **: $p < 0.01$, ***$p < 0.001$, ****$p < 0.0001$).

Additionally, we also evaluated FLT3 target engagement in Molm-14 cells to confirm the FLT3 inhibition seen in our preliminary kinase screen (Table 1). Cells were treated for 2 hours, harvested, and subsequently analyzed. Administration of HSK205 to Molm-14 cells led to a reduction of phosphorylated FLT3 (Fig. 5).

Many FLT3 inhibitors have been trialed in the clinic and some, such as gilteritinib, midostaurin and quizartinib, have been approved but on-target FLT3 mutations that reduce AML sensitivity to these drugs have been observed.[3] Thus, we evaluated HSK205 against Molm-14 cell lines that harbor resistant mutations commonly found in the clinic, FLT3-ITD-D835Y and F691L (Fig. 6). Remarkably, we found that HSK205 showed low nanomolar GI_{50} values against Molm-14-ITD-F691L (2.2 nM) and Molm-14-ITD-D835Y (4.3 nM).

Selectivity is important in the discovery of kinase inhibitors. It has been shown that FLT3 inhibitors, including those that have been FDA approved, commonly target additional kinases, such as KDR, PDGFR, c-KIT, and FGFR. Inhibition of these kinases can result in decreased tolerability and increased side effects. Specifically, it has been shown that co-inhibition of FLT3 and c-KIT can lead to myelosuppression and a high possibility of infection.[25] KDR, FGFR and PDGFR are all important for cardio function, and it is well known that targeting these cardiovascular-related kinases can result in low tolerability and increased side effects.[26–28] Additionally, our anti-target screening included CDK1, which has been demonstrated to lead to toxicity in normal proliferating cells.[29] We performed an in-lab kinase screening of our top compound, HSK205, against these anti-targets and compared to known haspin inhibitor, CHR-6494, and FDA-approved FLT3 inhibitor, gilteritinib (Fig. 7). HSK205 was screened at a concentration of 100 nM, roughly 500 times its FLT3 IC_{50}. Even at a high concentration, HSK205 showed minimal activity against these five anti-targets, which was similar to or lower than the activity of the well-tolerated gilteritinib.

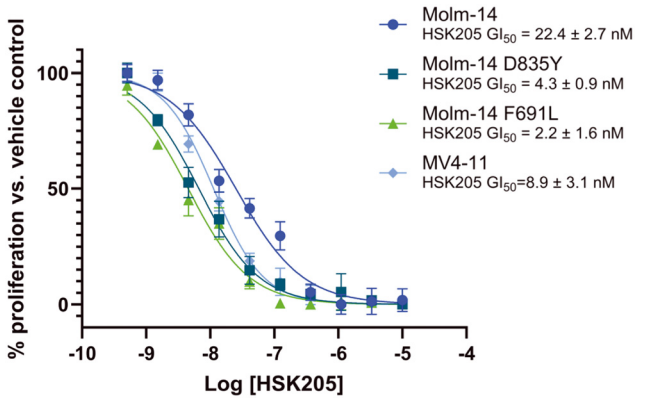

Fig. 6 Dose response curves. FLT3-driven AML cells were treated with varying concentrations of HSK205 for 72 h. Data was fitted to a non-linear regression equation using GraphPad Prism 9.0 software. Each data point represents the mean and error bars represent the SEM of triplicates.

To move compounds forward for further development, we routinely conduct DNA intercalation assays to eliminate compounds with high affinity for DNA. Although HSK205 contains polycyclic rings, which is typically seen as features that enhance DNA intercalation and unwanted toxicity,[30,31] it was determined HSK205 does not intercalate into DNA (Fig. 8). Under similar experimental conditions, mitoxantrone (a known DNA intercalator) was shown to associate with DNA (Fig. 8).

3. Conclusions

In this report we demonstrate that the recently reported protein kinase hinge binder, 3*H*-pyrazolo[4,3-*f*]quinoline, which is readily synthesized *via* a multicomponent reaction potently inhibit FLT3 and haspin. Our lead compound,

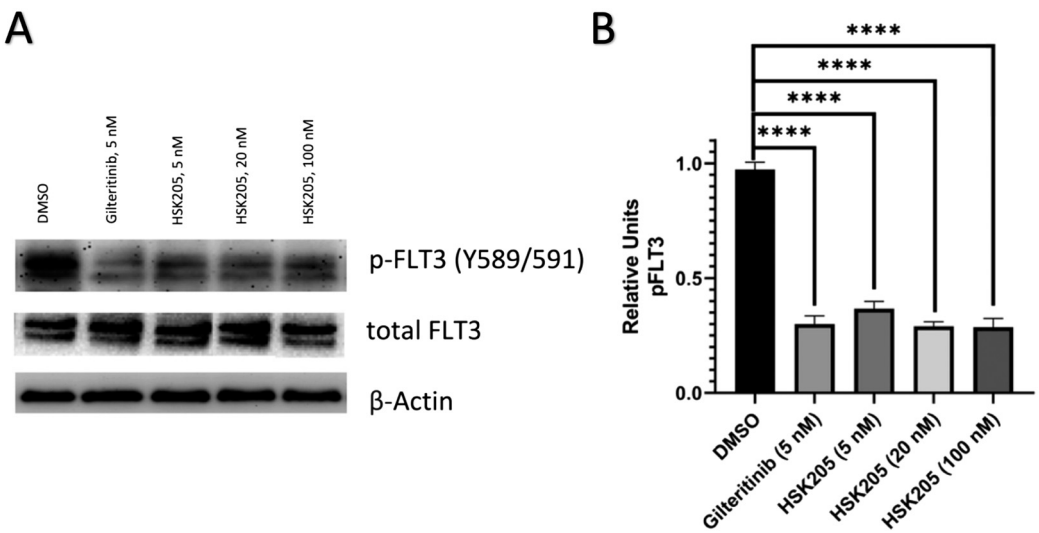

Fig. 5 Western blot analysis. (A) Molm-14 cells were treated with HSK205 (5, 20, or 100 nM) or control for 2 hours. Gilteritinib at 5 nM was used as a positive control. (B) Bands were quantified relative actin loading control. Values are reported as means of triplicates and error bars represent standard deviation ($p > 0.05$: NS, $p < 0.05$: *, $p < 0.01$: **, $p < 0.001$: ***, $p < 0.0001$: ****).

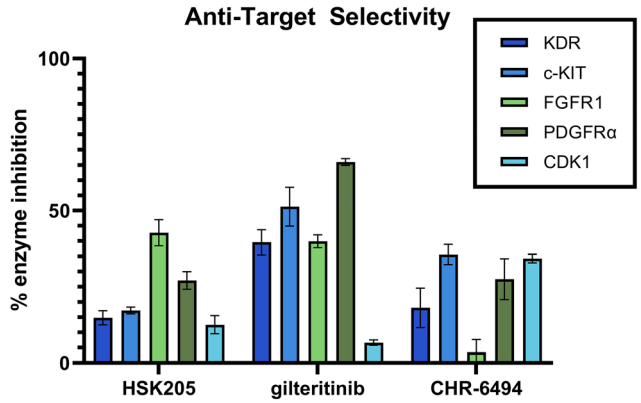

Fig. 7 Selectivity kinase inhibition for known anti-targets. HSK205 was screened at 100 nM against various specified kinases *via* the ADP Glo Kinase Assay. Known FLT3 inhibitor, gilteritinib, and known haspin inhibitor, CHR-6494, were used as positive controls. Results reported are means of triplicates and error bars represent standard deviation.

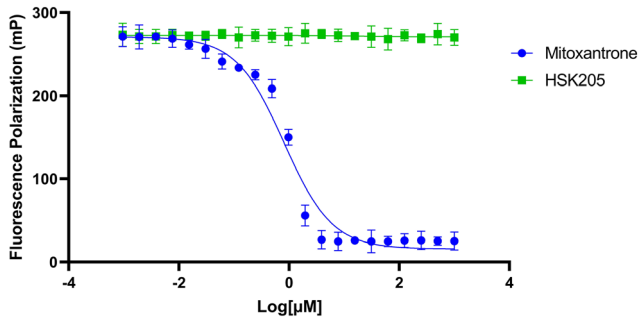

Fig. 8 DNA intercalation assay. Mitoxantrone was used as a positive control and DMSO as a negative control. Compounds, including mitoxantrone, were tested over a range of doses from 1 mM to 10 nM. Data was fitted to a nonlinear regression curve using GraphPad Prism 9.0 software. Each data point represents the mean of triplicates and error bars represent standard deviation.

HSK205, showed remarkable potencies *in vitro* and in cells against both haspin and FLT3. HSK205 inhibited the proliferation of AML cell lines harboring FLT3-ITD-D835Y or F691L, which are resistant to many of the reported FLT3 inhibitors. Additionally, HSK205 showed limited activity against select anti-targets, such as c-Kit and KDR.

4. Experimental section

4.1 Chemistry

Unless noted otherwise, all reagents and solvents were purchased from commercial sources and used as received. The ^{1}H and ^{13}C NMR spectra were obtained in DMSO-d_6 as solvent using a 500 MHz spectrometer or 800 MHz spectrometer with Me_4Si as an internal standard. Chemical shifts are reported in parts per million (δ) and are calibrated using residual undeuterated solvent as an internal reference. Data for ^{1}H NMR spectra are reported as follows: chemical shift (δ ppm) (multiplicity, coupling constant (Hz), integration). Multiplicities are reported as follows: s = singlet, d = doublet, t = triplet, q = quartet, m = multiplet, or combinations thereof. High resolution mass spectra (HRMS) were obtained using electron spray ionization (ESI) technique and a TOF mass analyzer. New compounds were characterized by ^{1}H NMR, ^{13}C NMR, and HRMS data, and purities of final compounds were reported using HPLC.

4.1.1. 4-(8,9,10,11-Tetrahydro-3*H*-pyrazolo[4,3-*a*]-phenanthridin-7-yl)benzoic acid (1). In a round bottom flask equipped with a stir bar, the appropriate indazole (1 eq.) and the appropriate aldehyde (1 eq.) were dissolved in ethanol. This mixture was refluxed at 120 °C for 2 hours, after which the appropriate ketone (2 eq.) and a catalytic amount of hydrochloric acid was added. This was allowed to stir at reflux for an additional 12 hours. The reaction solvent was evaporated using a rotary evaporator and purified *via* column chromatography with 10% methanol in ethyl acetate to yield an off-white solid (2.38 g, 69.4%). ^{1}H NMR (500 MHz, $(CD_3)_2SO$) δ 8.75 (s, 1H), 8.26 (d, J = 9.2 Hz, 1H), 8.19 (d, J = 9.2 Hz, 1H), 8.15–8.11 (m, 2H), 7.85–7.80 (m, 2H), 3.46 (t, J = 6.5 Hz, 2H), 2.76 (t, J = 6.1 Hz, 2H), 2.03 (dd, J = 6.0, 2.9 Hz, 2H), 1.83–1.76 (m, 2H). ^{13}C NMR (126 MHz, $(CD_3)_2SO$) δ 167.17, 151.31, 151.03, 140.41, 138.09, 137.05, 134.78, 132.69, 131.32, 130.42, 129.69, 123.45, 122.02, 120.11, 115.06, 30.67, 28.05, 21.85, 21.72. HRMS (ESI) m/z calcd for $C_{21}H_{17}N_3O_2$ $[M + H]^+$ 344.1393, found 344.1392.

4.1.2. 3-Fluoro-4-(8,9,10,11-tetrahydro-3*H*-pyrazolo[4,3-*a*]-phenanthridin-7-yl)benzoic acid (2). Following the same synthetic procedure as (**1**), the compound was obtained as an off-white solid (636 mg, 58.7%). ^{1}H NMR (500 MHz, $(CD_3)_2SO$) δ 8.64 (s, 1H), 8.06 (d, J = 22.2 Hz, 3H), 7.72 (d, J = 11.2 Hz, 1H), 7.63 (d, J = 8.1 Hz, 1H), 3.31 (t, J = 6.6 Hz, 2H), 2.76 (t, J = 6.2 Hz, 2H), 2.04–1.91 (m, 2H), 1.76 (q, J = 6.0 Hz, 2H). ^{13}C NMR (126 MHz, $(CD_3)_2SO$) δ 167.55, 165.09, 162.00, 159.95, 157.23, 150.10, 132.37, 131.56, 130.83, 126.27, 123.27, 123.14, 121.70, 120.78, 120.70, 118.99 (^{2}J = 22 Hz), 115.01, 30.42, 28.01, 21.88, 21.75. HRMS (ESI) m/z calcd for $C_{21}H_{16}FN_3O_2$ $[M + H]^+$ 362.1299, found 362.1300.

4.1.3. 2-Fluoro-4-(8,9,10,11-tetrahydro-3*H*-pyrazolo[4,3-*a*]-phenanthridin-7-yl)benzoic acid (3). Following the same synthetic procedure as (**1**), the compound was obtained as an off-white solid (556 mg, 51.3%). ^{1}H NMR (500 MHz, $(CD_3)_2SO$) δ 8.76 (d, J = 8.6 Hz, 1H), 8.16 (d, J = 14.3 Hz, 2H), 8.04 (t, J = 7.7 Hz, 1H), 7.67 (d, J = 11.1 Hz, 1H), 7.60 (d, J = 8.1 Hz, 1H), 3.47 (t, J = 6.6 Hz, 2H), 2.80 (t, J = 6.2 Hz, 2H), 2.05 (p, J = 6.0 Hz, 2H), 1.81 (p, J = 5.8 Hz, 2H). ^{13}C NMR (126 MHz, $(CD_3)_2SO$) δ 165.04, 162.04, 159.99, 150.59, 140.43, 138.54, 134.91, 132.33, 130.91, 126.13, 123.73, 123.41, 120.87, 119.44, 118.75 (^{2}J = 20 Hz), 115.32, 109.16, 30.48, 28.04, 21.99, 21.86. HRMS (ESI) m/z calcd for $C_{21}H_{16}FN_3O_2$ $[M + H]^+$ 362.1299, found 362.1301.

4.1.4. *N*-((1*H*-Imidazol-4-yl)methyl)-4-(8,9,10,11-tetrahydro-3*H*-pyrazolo[4,3-*a*]phenanthridin-7-yl)benzamide (4). In a 20 mL screw-capped vial equipped with a stir bar, the acid intermediate (1.3 eq.) and hexafluorophosphate azabenzotriazole tetramethyl uronium (HATU) (1.5 eq.) were sealed with a septum, air was removed *via* a vacuum pump,

and a nitrogen balloon was added to the reaction vessel to fill the vessel with an inert gas. To this reaction vial, anhydrous DMF (2 mL) and DIPEA (8 eq.) were added. This was heated at 60 °C for 30 min, and then the amine (1 eq.) was added. The reaction was allowed to stir at 60 °C overnight. The reaction solvent was evaporated using a rotary evaporator and purified *via* column chromatography using 1% ammonium hydroxide, 9% methanol and 90% ethyl acetate to afford an off-white solid (111 mg, 52.6%) ^{1}H NMR (500 MHz, $(CD_3)_2SO$) δ 8.81 (t, J = 5.6 Hz, 1H), 8.57 (s, 1H), 7.99 (d, J = 8.2 Hz, 2H), 7.94–7.76 (m, 2H), 7.67–7.63 (m, 2H), 7.62 (s, 1H), 6.98 (s, 1H), 4.46 (d, J = 5.6 Hz, 2H), 3.32 (t, J = 6.5 Hz, 2H), 2.76 (t, J = 6.1 Hz, 2H), 2.03–1.95 (m, 2H), 1.74 (dp, J = 9.1, 3.2, 2.6 Hz, 2H). ^{13}C NMR (126 MHz, $(CD_3)_2SO$) δ 166.39, 156.17, 144.01, 143.85, 142.53, 135.85, 135.21, 134.22, 129.65, 129.56, 129.42, 129.24, 127.47, 122.11, 117.09, 116.30, 36.81, 29.65, 28.83, 22.58, 22.50. HRMS (ESI) m/z calcd for $C_{25}H_{22}N_6O$ $[M + H]^+$ 423.1928, found 423.1911.

4.1.5. *N*-(2-(1*H*-Imidazol-1-yl)ethyl)-4-(8,9,10,11-tetrahydro-3*H*-pyrazolo[4,3-*a*]phenanthridin-7-yl)benzamide (5). Following the same synthetic procedure as (**4**), the compound was obtained as an off-white solid (84 mg, 38.5%) ^{1}H NMR (800 MHz, $(CD_3)_2SO$) δ 8.74 (t, J = 5.5 Hz, 1H), 8.57 (s, 1H), 7.93 (d, J = 7.8 Hz, 2H), 7.89 (d, J = 8.9 Hz, 1H), 7.86–7.80 (m, 1H), 7.65 (d, J = 7.8 Hz, 2H), 7.63 (s, 1H), 7.18 (s, 1H), 6.89 (s, 1H), 4.22 (t, J = 6.2 Hz, 2H), 3.63 (q, J = 5.9 Hz, 2H), 2.78 (t, J = 6.2 Hz, 2H), 2.06–1.99 (m, 2H), 1.80–1.73 (m, 2H). ^{13}C NMR (201 MHz, $(CD_3)_2SO$) δ 166.82, 156.07, 144.98, 144.06, 142.49, 138.75, 137.79, 136.28, 133.87, 129.51, 129.39, 128.73, 127.30, 126.85, 119.97, 118.38, 116.37, 114.52, 45.60, 40.91, 29.60, 28.76, 22.50, 22.41. HRMS (ESI) m/z calcd for $C_{26}H_{24}N_6O$ $[M + H]^+$ 437.2084, found 437.2081.

4.1.6. *N*-((1*H*-Imidazol-2-yl)methyl)-4-(8,9,10,11-tetrahydro-3*H*-pyrazolo[4,3-*a*]phenanthridin-7-yl)benzamide (6). Following the same synthetic procedure as (**4**), the compound was obtained as an off-white solid (65 mg, 30.8%). ^{1}H NMR (800 MHz, $(CD_3)_2SO$) δ 9.17 (t, J = 5.9 Hz, 1H), 8.57 (s, 1H), 8.07 (d, J = 7.8 Hz, 2H), 7.89 (d, J = 9.0 Hz, 1H), 7.82 (d, J = 9.3 Hz, 1H), 7.65 (d, J = 7.8 Hz, 2H), 6.93 (s, 2H), 4.56 (d, J = 5.6 Hz, 2H), 2.77 (t, J = 6.3 Hz, 2H), 2.00 (q, J = 6.8, 6.3 Hz, 2H), 1.75 (p, J = 5.6 Hz, 2H). ^{13}C NMR (201 MHz, $(CD_3)_2SO$) δ 166.48, 156.04, 146.73, 145.52, 144.05, 143.70, 142.46, 138.80, 136.15, 133.75, 129.47, 129.33, 129.16, 127.57, 127.50, 122.02, 119.08, 116.22, 114.55, 37.50, 29.58, 28.75, 22.49, 22.41. HRMS (ESI) m/z calcd for $C_{25}H_{22}N_6O$ $[M + H]^+$ 423.1927, found 423.1926.

4.1.7. *N*-((1-Methyl-1*H*-imidazol-2-yl)methyl)-4-(8,9,10,11-tetrahydro-3*H*-pyrazolo[4,3-*a*]phenanthridin-7-yl)benzamide (7). Following the same synthetic procedure as (**4**), the compound was obtained as a pale-yellow solid (68 mg, 31.2%). ^{1}H NMR (500 MHz, $(CD_3)_2SO$) δ 8.56 (s, 1H), 8.37 (d, J = 4.3 Hz, 3H), 8.16 (d, J = 8.3 Hz, 3H), 7.04 (d, J = 13.1 Hz, 1H), 6.78 (d, J = 18.9 Hz, 1H), 4.56 (d, J = 5.3 Hz, 2H), 3.68 (s, 3H), 3.58 (s, 2H) 2.77 (t, J = 6.2 Hz, 3H), 1.88 (dp, J = 127.7, 5.7 Hz, 6H), 1.23 (dd, J = 14.7, 7.0 Hz, 2H). ^{13}C NMR (126 MHz, $(CD_3)_2SO$) δ 166.48, 156.10, 147.20, 144.21, 142.53, 139.90, 134.92, 133.82, 129.52, 129.41, 129.19, 127.72, 127.58, 126.87, 122.20, 119.24, 36.04, 32.94, 29.66, 28.80, 22.59, 22.52. HRMS (ESI) m/z calcd for $C_{26}H_{25}N_6O$ $[M + H]^+$ 437.2084, found 437.2081.

4.1.8. *N*-((4*H*-1,2,4-Triazol-3-yl)methyl)-4-(8,9,10,11-tetrahydro-3*H*-pyrazolo[4,3-*a*]phenanthridin-7-yl)benzamide (8). Following the same synthetic procedure as (**4**), the compound was obtained as an off-white solid (79 mg, 37.4%). ^{1}H NMR (500 MHz, $(CD_3)_2SO$) δ 8.58 (s, 1H), 8.43–8.06 (m, 2H), 8.01 (d, J = 7.8 Hz, 2H), 7.84 (q, J = 9.1 Hz, 2H), 7.65 (d, J = 7.8 Hz, 2H), 4.61 (d, J = 5.6 Hz, 2H), 3.34 (d, J = 13.1 Hz, 2H), 2.78 (t, J = 6.1 Hz, 2H), 1.89 (dp, J = 125.7, 6.1 Hz, 4H). ^{13}C NMR (126 MHz, $(CD_3)_2SO$) δ 166.66, 161.54, 156.17, 148.63, 144.20, 143.89, 142.55, 133.95, 129.66, 129.41, 129.24, 127.56, 122.14, 119.78, 116.29, 36.76, 29.66, 28.81, 22.59, 22.53. HRMS (ESI) m/z calcd for $C_{24}H_{21}N_7O$ $[M + H]^+$ 424.1880, found 424.1877.

4.1.9. *N*-((1*H*-Imidazol-2-yl)methyl)-3-fluoro-4-(8,9,10,11-tetrahydro-3*H*-pyrazolo[4,3-*a*]phenanthridin-7-yl)benzamide (9). Following the same synthetic procedure as (**4**), the compound was obtained as an off-white solid (109 mg, 49.5%). ^{1}H NMR (500 MHz, $(CD_3)_2SO$) δ 8.59 (s, 1H), 7.93–7.78 (m, 4H), 7.57 (t, J = 7.6 Hz, 1H), 7.16 (s, 2H), 4.65 (d, J = 5.5 Hz, 2H), 3.35 (t, J = 6.5 Hz, 2H), 2.62 (t, J = 6.2 Hz, 2H), 2.04–1.74 (m, 4H). ^{13}C NMR (126 MHz, $(CD_3)_2SO$) δ 165.63, 161.85, 159.52 (^1J = 246.4 Hz), 151.59, 151.13, 145.34, 144.18, 143.97, 142.50, 136.45, 131.98, 131.87, 129.97, 129.47, 129.06, 124.10, 122.51, 121.17, 116.22, 115.16 (^2J = 20 Hz), 36.92, 29.47, 27.37, 22.56, 22.17. HRMS (ESI) m/z calcd for $C_{25}H_{21}FN_6O$ $[M + H]^+$ 441.1833, found 441.1830.

4.1.10. *N*-((1*H*-Tetrazol-5-yl)methyl)-4-(8,9,10,11-tetrahydro-3*H*-pyrazolo[4,3-*a*]phenanthridin-7-yl)benzamide (10). To a solution of the alkyne (1 eq.) in DMF (2 mL) and water (0.5 mL) was added TMS-azide (2 eq.). Catalytic amount of copper sulfide pentahydrate and sodium ascorbate added. The reaction mixture was allowed to stir at 100 °C overnight. The reaction solvent was evaporated using a rotary evaporator, the residue was diluted with ethyl acetate, washed with water, and dried over sodium sulfate. It was then purified *via* column chromatography with 90% ethyl acetate and 10% hexanes to afford an off-white solid (36 mg, 34%). ^{1}H NMR (500 MHz, $(CD_3)_2SO$) δ 9.43 (dt, J = 33.1, 5.5 Hz, 1H), 8.79 (d, J = 3.9 Hz, 1H), 8.33–8.08 (m, 4H), 7.83 (dd, J = 8.1, 3.9 Hz, 2H), 4.82 (d, J = 5.6 Hz, 2H), 3.50 (t, J = 6.2 Hz, 2H), 2.78 (t, J = 6.2 Hz, 2H), 2.15–1.98 (m, 2H), 1.82 (ddt, J = 11.9, 9.4, 4.1 Hz, 2H). ^{13}C NMR (126 MHz, $(CD_3)_2SO$) δ 166.55, 155.31, 151.46, 140.50, 137.36, 135.41, 131.33, 130.29, 130.13, 128.06, 128.01, 123.41, 122.54, 120.16, 117.93, 115.22, 33.87, 30.66, 28.29, 28.13, 21.92, 21.80. HRMS (ESI) m/z calcd for $C_{23}H_{20}N_8O$ $[M + H]^+$ 425.1833, found 425.1831.

4.1.11. *N*-((1*H*-Imidazol-2-yl)methyl)-2-fluoro-4-(8,9,10,11-tetrahydro-3*H*-pyrazolo[4,3-*a*]phenanthridin-7-yl)benzamide (11). Following the same synthetic procedure as (**4**), the compound was obtained as an off-white solid (87 mg, 39.5%). ^{1}H NMR (500 MHz, $(CD_3)_2SO$) δ 8.82 (q, J = 4.9 Hz, 1H), 8.55 (s, 1H), 7.83 (dq, J = 22.1, 9.0, 7.4 Hz, 3H), 7.50 (t, J = 10.4 Hz, 2H), 6.97 (s, 2H), 4.55 (d, J = 5.6 Hz, 2H), 3.25 (t, J = 6.7 Hz, 2H), 2.76 (t, J = 6.1 Hz, 2H), 1.96 (p, J = 6.5, 6.1 Hz, 2H), 1.72 (p, J = 5.7 Hz, 2H). ^{13}C

NMR (126 MHz, $(CD_3)_2SO$) δ 164.00, 161.89, 160.52 (^1J = 249.4 Hz), 154.65, 149.62, 145.80, 145.73, 145.06, 143.72, 142.71, 138.50, 130.58, 129.58, 129.18, 125.69, 122.93, 122.82, 122.25, 117.29 (^2J = 23 Hz), 116.18, 37.66, 29.62, 28.70, 22.48, 22.40. HRMS (ESI) *m*/*z* calcd for $C_{25}H_{21}FN_6O$ $[M + H]^+$ 441.1873, found 441.1837.

4.1.12. *N*-((1*H*-Pyrrol-3-yl)methyl)-4-(8,9,10,11-tetrahydro-3*H*-pyrazolo[4,3-*a*]phenanthridin-7-yl)benzamide (12). Following the same synthetic procedure as (**4**), the compound was obtained as a light brown solid (77 mg, 36.5%). ^{1}H NMR (500 MHz, $(CD_3)_2SO$) δ 8.47 (s, 1H), 8.01 (d, J = 8.0 Hz, 2H), 7.79 (q, J = 9.1 Hz, 2H), 7.60 (d, J = 7.9 Hz, 2H), 6.74 (t, J = 2.1 Hz, 1H), 6.67 (q, J = 2.4 Hz, 1H), 6.08 (q, J = 2.3 Hz, 1H), 4.41 (d, J = 5.6 Hz, 2H), 3.53 (p, J = 6.6 Hz, 2H), 3.17 (t, J = 6.4 Hz, 2H), 1.89 (q, J = 7.6, 6.3 Hz, 2H), 1.63 (p, J = 6.1, 5.7 Hz, 2H). ^{13}C NMR (126 MHz, $(CD_3)_2SO$) δ 166.30, 165.17, 162.82, 156.02, 143.84, 143.75, 142.45, 134.41, 129.52, 129.36, 129.11, 127.37, 127.01, 121.99, 120.98, 118.03, 116.28, 116.22, 107.90, 54.09, 36.02, 22.38, 22.33, 12.65. HRMS (ESI) *m*/*z* calcd for $C_{26}H_{23}N_5O$ $[M + H]^+$ 422.1981, found 422.1971.

4.1.13. 4-(8,9,10,11-Tetrahydro-3*H*-pyrazolo[4,3-*a*]-phenanthridin-7-yl)-*N*-(thiazol-2-ylmethyl)benzamide (13). Following the same synthetic procedure as (**4**), the compound was obtained as an off-white solid (65 mg, 29.8%). ^{1}H NMR (500 MHz, $(CD_3)_2SO$) δ 9.40 (t, J = 6.0 Hz, 1H), 8.57 (s, 1H), 8.07–7.98 (m, 2H), 7.90–7.78 (m, 2H), 7.73 (d, J = 3.3 Hz, 1H), 7.72–7.65 (m, 2H), 7.61 (d, J = 3.3 Hz, 1H), 4.80 (d, J = 5.9 Hz, 2H), 3.33 (s, 2H), 2.78 (t, J = 6.1 Hz, 2H), 2.05–1.96 (m, 2H), 1.84–1.71 (m, 2H). ^{13}C NMR (126 MHz, $(CD_3)_2SO$) δ 169.89, 166.81, 156.08, 144.47, 142.64, 142.58, 136.40, 133.52, 129.66, 129.63, 129.29, 127.52, 127.07, 122.13, 120.49, 114.52, 41.53, 29.67, 28.83, 22.58, 22.51. HRMS (ESI) *m*/*z* calcd for $C_{25}H_{21}N_5OS$ $[M + H]^+$ 440.1545, found 440.1547.

4.1.14. *N*-((4-Methyl-1*H*-imidazol-2-yl)methyl)-4-(8,9,10,11-tetrahydro-3*H*-pyrazolo[4,3-*a*]phenanthridin-7-yl)benzamide (14). Following the same synthetic procedure as (**4**), the compound was obtained as an off-white solid (89 mg, 40.7%). ^{1}H NMR (500 MHz, $(CD_3)_2SO$) δ 9.01 (t, J = 5.7 Hz, 1H), 8.57 (s, 1H), 8.05–7.99 (m, 2H), 7.89–7.80 (m, 2H), 7.68–7.63 (m, 2H), 6.63–6.58 (m, 1H), 4.46 (d, J = 5.7 Hz, 2H), 2.77 (t, J = 6.1 Hz, 2H), 2.09 (d, J = 1.0 Hz, 3H), 2.07 (s, 1H), 2.01 (dd, J = 7.8, 3.9 Hz, 2H), 1.97 (s, 1H), 1.75 (dd, J = 7.6, 4.2 Hz, 2H). ^{13}C NMR (126 MHz, $(CD_3)_2SO$) δ 166.47, 156.23, 149.06, 144.60, 144.08, 143.78, 142.59, 138.74, 136.44, 133.83, 132.46, 129.67, 129.44, 127.61, 122.02, 116.46, 114.56, 105.50, 60.23, 37.63, 29.71, 28.87, 22.58, 14.56. HRMS (ESI) *m*/*z* calcd for $C_{26}H_{24}N_6O$ $[M + H]^+$ 437.2079, found 437.2083.

4.1.15. *N*-(2-(1*H*-Imidazol-2-yl)ethyl)-4-(8,9,10,11-tetrahydro-3*H*-pyrazolo[4,3-*a*]phenanthridin-7-yl)benzamide (15). Following the same synthetic procedure as (**4**), the compound was obtained as an off-white solid (73 mg, 33.4%). ^{1}H NMR (500 MHz, $(CD_3)_2SO$) δ 8.63 (t, J = 5.6 Hz, 1H), 8.57 (s, 1H), 7.93–7.89 (m, 2H), 7.87–7.77 (m, 2H), 7.64 (d, J = 8.3 Hz, 2H), 7.16 (d, J = 21.5 Hz, 1H), 6.90 (d, J = 10.4 Hz, 1H), 4.21 (t, J = 6.1 Hz, 2H), 3.63 (q, J = 5.9 Hz, 2H), 3.42 (q, J = 6.0 Hz, 2H), 2.76 (t, J = 6.1 Hz, 2H), 1.99 (ddd, J = 15.1, 7.5, 4.5 Hz, 2H), 1.73 (ddd, J = 9.0, 7.2, 4.2 Hz, 2H). ^{13}C NMR (126 MHz, $(CD_3)_2SO$) δ 166.94, 161.91, 156.11, 144.18, 143.82, 142.54, 137.83, 134.00, 129.65, 129.49, 129.24, 128.72, 128.67, 127.35, 122.11, 120.11, 119.92, 116.35, 45.82, 38.81, 29.65, 28.83, 22.57, 22.49. HRMS (ESI) *m*/*z* calcd for $C_{26}H_{24}N_6O$ $[M + H]^+$ 437.2084, found 437.2070.

4.2 Biological evaluation

4.2.1. Kinase assay. The ADP-Glo Kinase Assay Kit (Promega) was used to determine inhibition of haspin. Kinase Buffer (SignalChem Cat# K01-09; 25 mM MOPS, pH 7.2, 12.5 mM β-glycerol-phosphate, 25 mM MgCl2, 2 mM EDTA) was supplemented with DTT (0.2 mM) and BSA (40 μg mL^{-1}) immediately prior to use. Reaction volumes of 5 μL containing 9 ng μL^{-1} kinase, 10 μM ATP, 50 nM inhibitor, and the appropriate peptide substrate (20 μM) were incubated for 3 hours, and then quenched with an equal volume (5 μL) of GLO reagent. After 40 min, 10 μL DET reagent was added and incubated for 1 hour before visualization on a Cytation™ 5 Cell Imaging Multi-Mode Reader (BioTek).

4.2.2. Cell cultures. MV4-11 cells were obtained from Cell Lines Service and were cultivated according to the provider's instructions. MOLM-14, MOLM-14 (D835Y), and MOLM-14 (F691L) were generously provided by Prof. Neil Shah (Department of Medicine, UCSF, San Francisco, CA). Cells were cultured to confluence in RPMI supplemented with 10% fetal bovine serum and 1× penicillin–streptomycin (Gibco™). Cells were plated at 5000 cells per well in 96 well plates. After 24-hour incubation at 37 °C in a 5% CO_2 incubator, compounds diluted in the same media were added to the indicated final concentration and allowed to incubate at 37 °C in a 5% CO_2 incubator for 72 hours. Viability was determined using CellTiter-Blue® Cell Viability Assay (Promega) with absorbance readings at 570 nm performed on a Cytation™ 5 Cell Imaging Multi-Mode Reader (BioTek) 3 hours after addition. Appropriate vehicle and cell-free controls were included. GI_{50} readings were confirmed by two scientists on two separate days.

4.2.3. Immunoblotting. MOLM-14 cells were incubated with various concentrations of compound as specified. Cells were collected and lysed, and protein concentrations were quantified relative to BSA standards. After protein denaturation, proteins were separated *via* SDS-PAGE electrophoresis and transferred to NC membranes. After blocking, overnight incubation with specific primary antibodies, and room temperature incubation for 2 hours with peroxidase-conjugated secondary antibodies, peroxidase activity was detected with SuperSignal West Pico reagents (Thermo Scientific) using a CCD camera LAS-4000 (Fujifilm). Bands were normalized using housekeeping gene, actin. Values reported represent the means of triplicates and error bars represent SD. All specific antibodies were purchased from Cell Signaling.

4.3 Molecular docking

The crystal structure for haspin (PDB: 2WB8) was downloaded from the Protein Data Bank and edited to

remove any existing bound ligand within the protein active site. Two-dimensional ligands were built in ChemDraw 21.0.0 and were transferred to three-dimensional mol2 files using OpenBabel. Docking was performed using the Glide software by Schrödinger. Waters were removed before docking into haspin. Docking trial validation for the haspin kinase was based off the previously generated docking pose of HSD972. Visualization was performed through PyMol and Maestro.

Author contributions

HOS provided conceptualization. Investigation was done by ALK and NRB. ALK wrote original draft. Writing, review, and editing was performed by NRB and HOS. HOS provided funding acquisition and supervision.

Conflicts of interest

HOS holds shares in KinaRx Inc., a company with interest in oncology.

Acknowledgements

This study was supported by the National Institutes of Health (1R01CA267978-01) and Purdue University.

Notes and references

1 R. L. Siegel, K. D. Miller, H. E. Fuchs and A. Jemal, *Ca-Cancer J. Clin.*, 2022, **72**, 7–33.
2 M. Lin and B. Chen, *Drug Des., Dev. Ther.*, 2018, **12**, 1009–1017.
3 S. Scholl, M. Fleischmann, U. Schnetzke and F. H. Heidel, *Cells*, 2020, **9**, 2493.
4 A. S. Alotaibi, M. Yilmaz, R. Kanagal-Shamanna, S. Loghavi, T. M. Kadia, C. D. DiNardo, G. Borthakur, M. Konopleva, S. A. Pierce, S. A. Wang, G. Tang, V. Guerra, B. Samra, N. Pemmaraju, E. Jabbour, N. J. Short, G. C. Issa, M. Ohanian, G. Garcia-Manero, K. N. Bhalla, K. P. Patel, K. Takahashi, M. Andreeff, J. E. Cortes, H. M. Kantarjian, F. Ravandi and N. Daver, *Cancer Discovery*, 2021, **2**, 125–134.
5 P. M. Kasi, M. R. Litzow, M. M. Patnaik, S. K. Hashmi and N. Gangat, *Leuk. Res. Rep.*, 2016, **5**, 7–10.
6 L. K. Schmalbrock, A. Dolnik, S. Cocciardi, E. SträngStr, F. Theis, N. Jahn, E. Panina, T. J. Bïatte, J. Herzig, S. Skambraks, F. G. Rücker, V. I. Gaidzik, P. Paschka, W. Fiedler, H. R. Salih, G. Wulf, T. Schroeder, R. F. Schlenk, F. Thol, M. Heuser, R. A. Larson, A. Ganser, H. G. Stunnenberg, S. Minucci, R. M. Stone, C. D. Bloomfield and L. Bullinger, *Blood*, 2021, **137**, 3093–3104.
7 K. A. Minson, C. C. Smith, A. B. Lee-Sherick, D. DeRyckere, E. Lasater, A. A. Hill, X. Wang, S. V. Frye, H. S. Earp, N. P. Shah and D. K. Graham, *Blood*, 2014, **124**, 3757.
8 S. C. Yen, L. C. Chen, H. L. Huang, W. C. HuangFu, Y. Y. Chen, T. Eight Lin, S. T. Lien, H. J. Tseng, T. Y. Sung, J. H. Hsieh, W. J. Huang, S. L. Pan and K. C. Hsu, *Bioorg. Chem.*, 2022, **121**, 105675.
9 K. C. Goh, W. C. Ong, C. Hu, A. L. Liang, W. Stunkel, Y. C. Tan, K. Sangthongpitag, S. K. Goh, Z. Q. Bonday, A. D. William, B. W. Dymock, E. Kantharaj and J. M. Wood, *Blood*, 2007, **110**, 1593.
10 N. Dayal, C. Opoku-Temeng, D. E. Hernandez, M. A. Sooreshjani, B. A. Carter-Cooper, R. G. Lapidus and H. O. Sintim, *Future Med. Chem.*, 2018, **10**, 823–835.
11 W. Czardybon, R. Windak, A. Gołas, M. Gałęzowski, A. Sabiniarz, I. Dolata, M. Salwińska, P. Guzik, M. Zawadzka, E. Gabor-Worwa, B. Winnik, M. Żurawska, E. Kolasińska, E. Wincza, M. Bugaj, M. Danielewicz, E. Majewska, M. Mazan, G. Dubin, M. Noyszewska-Kania, E. Jabłońska, M. Szydłowski, T. Sewastianik, B. Puła, A. Szumera-Ciećkiewicz, M. Prochorec-Sobieszek, E. Mądro, E. Lech-Marańda, K. Warzocha, J. Tamburini, P. Juszczyński and K. Brzózka, *Oncotarget*, 2018, **9**, 16917–16931.
12 D. Taussig, J. O'Nions, M. Jongen-Lavrencic, J. J. Janssen, D. C. de Leeuw, P. T. Tan, S. Brook, K. Stoddart, H.-T. Arkenau and G. Fisher, *Blood*, 2022, **140**, 6222–6223.
13 M. U. Tariq, M. Furqan, H. Parveen, R. Ullah, M. Muddassar, R. S. Z. Saleem, V. Bavetsias, S. Linardopoulos and A. Faisal, *Br. J. Cancer*, 2021, **125**, 966–974.
14 Z. Li, X. Wang, J. Eksterowicz, M. W. Gribble Jr, G. Q. Alba, M. Ayres, T. J. Carlson, A. Chen, X. Chen, R. Cho, R. V. Connors, M. DeGraffenreid, J. T. Deignan, J. Duquette, P. Fan, B. Fisher, J. Fu, J. N. Huard, J. Kaizerman, K. S. Keegan, C. Li, K. Li, Y. Li, L. Liang, W. Liu, S. E. Lively, M.-C. Lo, J. Ma, D. L. McMinn, J. T. Mihalic, K. Modi, R. Ngo, K. Pattabiraman, D. E. Piper, C. Queva, M. L. Ragains, J. Suchomel, S. Thibault, N. Walker, X. Wang, Z. Wang, M. Wanska, P. M. Wehn, M. F. Weidner, A. J. Zhang, X. Zhao, A. Kamb, D. Wickramasinghe, K. Dai, L. R. McGee and J. C. Medina, *J. Med. Chem.*, 2014, **57**, 3430–3449.
15 N. G. Amoussou, A. Bigot, C. Roussakis and J. M. H. Robert, *Drug Discovery Today*, 2018, **23**, 409–415.
16 M. Liu, S. A. Stoner, A. G. Davis and D.-E. Zhang, *Blood*, 2022, **140**, 2997–2998.
17 N. Dayal, E. Řezníčková, D. E. Hernandez, M. Peřina, S. Torregrosa-Allen, B. D. Elzey, J. Škerlová, H. Ajani, S. Djukic, V. Vojáčková, M. Lepšík, P. Řezáčová, V. Kryštof, R. Jorda and H. O. Sintim, *J. Med. Chem.*, 2021, **64**, 10981–10996.
18 N. Dayal, C. Opoku-Temeng, D. E. Hernandez, M. A. Sooreshjani, B. A. Carter-Cooper, R. G. Lapidus and H. O. Sintim, *Future Med. Chem.*, 2018, **10**, 823–835.
19 N. Dayal, C. G. Mikek, D. Hernandez, G. A. Naclerio, E. F. Yin Chu, B. A. Carter-Cooper, R. G. Lapidus and H. O. Sintim, *Eur. J. Med. Chem.*, 2019, **180**, 449–456.
20 C. Opoku-Temeng, N. Dayal, D. E. Hernandez, N. Naganna and H. O. Sintim, *Chem. Commun.*, 2018, **54**, 4521–4524.
21 C. Opoku-Temeng, N. Dayal, M. Aflaki Sooreshjani and H. O. Sintim, *Bioorg. Chem.*, 2018, **78**, 418–426.
22 P. L. Nguyen, C. H. Lee, H. Lee and J. Cho, *Antioxidants*, 2022, **11**, 117.
23 J. Eswaran, D. Patnaik, P. Filippakopoulos, F. Wang, R. L. Stein, J. W. Murray, J. M. G. Higgins and S. Knapp, *Proc. Natl. Acad. Sci. U. S. A.*, 2009, **106**, 20198–20203.

24 P. Shah and A. D. Westwell, *J. Enzyme Inhib. Med. Chem.*, 2007, **22**, 527–540.
25 A. A. Warkentin, M. S. Lopez, E. A. Lasater, K. Lin, B.-L. He, A. Y. Leung, C. C. Smith, N. P. Shah and K. M. Shokat, *eLife*, 2014, **3**, e03445.
26 A. Kommalapati, S. H. Tella, M. Borad, M. Javle and A. Mahipal, *Cancers*, 2021, **13**, 2968.
27 T. Force, D. S. Krause and R. A. Van Etten, *Nat. Rev. Cancer*, 2007, **7**, 332–344.
28 R. M. Touyz and J. Herrmann, *npj Precis. Oncol.*, 2018, **2**, 13.
29 R. Prevo, G. Pirovano, R. Puliyadi, K. J. Herbert, G. Rodriguez-Berriguete, A. O'Docherty, W. Greaves, W. G. McKenna and G. S. Higgins, *Cell Cycle*, 2018, **17**, 1513–1523.
30 F. P. Guengerich, Base Intercalation in DNA, in *Molecular Life Sciences*, ed. R. D. Wells, J. S. Bond, J. Klinman and B. S. S. Masters, *Molecular Life Sciences*, Springer, New York, NY, 2018, DOI: **10.1007/978-1-4614-1531-2_432**.
31 K. Gurova, *Future Oncol.*, 2009, **5**, 1685–1704.